IEEE Photonics Journal
An IEEE Photonics Society Publication

Open Access

Effective Mass Sensing Using Optomechanically Induced Transparency in Microresonator System

Volume 9, Number 1, February 2017

Yong-Pan Gao
Tie-Jun Wang
Cong Cao
Si-Chen Mi
Daquan Yang
Yong Zhang
Chuan Wang

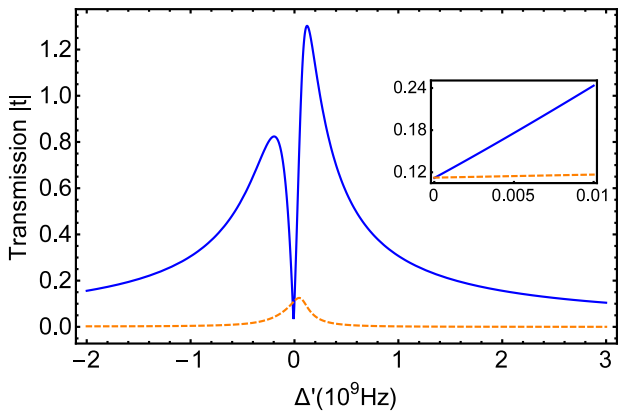

DOI: 10.1109/JPHOT.2016.2639045
1943-0655

Effective Mass Sensing Using Optomechanically Induced Transparency in Microresonator System

Yong-Pan Gao,[1] Tie-Jun Wang,[1] Cong Cao,[1] Si-Chen Mi,[1] Daquan Yang,[2] Yong Zhang,[3] and Chuan Wang[1]

[1]School of Science and the State Key Laboratory of Information Photonics and Optical Communications, Beijing University of Posts and Telecommunications, Beijing 100876, China
[2]State Key Laboratory of Information Photonics and Optical Communications, School of Information and Communication Engineering, Beijing University of Posts and Telecommunications, Beijing 100876, China
[3]School of Science, Beijing University of Posts and Telecommunications, Beijing 100876, China

DOI:10.1109/JPHOT.2016.2639045

Manuscript received November 15, 2016; accepted December 7, 2016. Date of publication December 13, 2016; date of current version January 4, 2017. This work was supported in part by the National Natural Science Foundation of China under Grant 61622103, Grant 61501053, Grant 61471050, and Grant 11404031; in part by the Fok Ying-Tong Education Foundation for Young Teachers in the Higher Education Institutions of China under Grant 151063; and in part by the Open Research Fund Program of the State Key Laboratory of Low-Dimensional Quantum Physics, Tsinghua University, under Grant KF201610. Corresponding authors: C. Wang (e-mail: wangchuan@bupt.edu.cn).

Abstract: Detecting and weighing individual nanoparticles is an important approach to studying the behavior and properties of single particles. Here, we illustrate an effective mass sensing scheme using optomechanical resonator system. Based on the optomechanically induced transparency phenomenon, a Stokes' field reference approach is used to sense the mass of the particle on the microresonator. The field intensity of the transmission field will be changed by the effect of the particle, which avoids the limits of decay-induced spectral width in the resonance shift detection. Exploiting the perturbation method, we theoretically evaluated the dynamical behavior of the system and achieved femtogram-level mass sensing without the need for high cavity Q-value, as well as strong coupling strength in the optomechanical system.

Index Terms: Mass sensing, optomechanically induced transparency, microresonator.

1. Introduction

Mass sensing, which is used to weigh the external nanoparticle and molecules with tiny mass, is a hot spot in recent researches. To date, most of the mass sensing schemes are based on electrical or optical equipments. The electrical schemes are usually based on the nano-electromechanical system (NEMS) [1]–[4]. In particular, the NEMS is generally constructed by a sorbet coated cantilever or bridge; when a single particle is deposited on the system, it would induce an intrinsic frequency shift result from the changement of the effective mass. On the basis of this frequency shift, the mass change induced by the nanoparticle can be read out. To our knowledge, the precision of the electrical sensing scheme is approaching the attogram level in vacuum [5]. However, the ohmic

effect and other intrinsic energy loss in the electric circuitry will broaden the electrical response spectrum and finally affect the sensitivity of the mass detection during the frequency measurement. Compared with the traditional electrical methods, optical sensors do not require on-chip power and allows for remote sensing via free-space or optical fibers [6]. In particular, by exploiting the whispering-gallery-mode (WGM) resonators as the platform, various schemes of particle detection have been realized. For example, Zhu *et al.* realized the single nanoparticle sensing using silica optical microtoroids in 2010 [7]. Later, by exploiting the Erbium doped microcavities, He *et al.* investigated the single viruses and nanoparticles sensing using whispering gallery mode microlaser [8]. Further by using Raman effect, the sensitivity and precision are improved [9], [10]. During the past decades, various important progress on this field has been made [11]–[14]. Also, with the development of cavity optomechanics, the optical pump-probe response becomes a popular issue in the study of optomechanical system [15]–[17]. Exploiting the mechanical system, various studies and applications in optical and electrical systems have been presented, such as the optomechanics [18]–[20], nanomechanics [21]–[23], and so on.

The mechanical resonator based mass sensing relies on the resonant frequency-shift due to the increment of the mass value. Over the past few decades, there have been various experiments progress on the branches of particle sensing and mass sensing using optical and mechanical systems. In 2013, Chaste *et al.* experimentally investigated the mass sensing using carbon nanotubes with a resolution of 1 zg level [24]. Based on the nanomechanical system, Jensen *et al.* [25] demonstrated a nanoscale mechanical resonator for atomic mass sensing with sensitivity of $13ag/\sqrt{Hz}$. Then, the mass sensor operated in the nonlinear optical domain was demonstrated in the toroidal nanocavity optomechanically system [26]. Later, the sub-picogram mass sensing and measurement with an optomechanical oscillator was experimentally presented [27]. After that, sensors using micro fluidic optomechanical resonators at the picogram level in liquid environment was experiment achieved [28]. Recently, a coupled double-cavity optomechanical system was also theoretical exploited to sense the mass at picogram level [29]. It is worthwhile to note that these schemes have achieved mass sensing based on the direct frequency shift detection, which means that the accuracy of the system will be limited by the spectra linewidth, which could be called inter-band sensing.

In this study, we propose an efficient mass sensing scheme to weigh the external nanoparticle deposited onto the surface of a mechanical resonator using pump-probe response of the optomechanical system under the condition of optomechanically induced transparency (OMIT) [30]–[34]. OMIT is the analogue of electromagnetically induced transparency (EIT) [35]–[37] based in the optomechanics. In the pump-probe driving progress of cavity optomechanical system, the four-wave mixing (FWM) [38]–[41] would produce the stokes field, which shows different transparency characteristics compared with the OMIT field when the mechanical resonator exhibits a slight frequency change.

Based on the change of the transparency characteristics, we find that the mass of the added subject can be read out from the output field intensity. Compared with the previous schemes based on the detection of frequency shift, the present scheme avoids the effect of the cross-talk in the spectrum. We can therefore read out the frequency even if the full width half maximum (FWHM) far outweighs than the frequency shift. In other words, this relative intensity method enable us to achieve sensing inner the transmission spectrum. Then, we can overcome the limit of the spectra line width of previous scheme mentioned in above paragraph. Therefore, our scheme will be more accurate compare with the frequency shift detection methods. Moreover, the most important issue is the unavoidable dissipation in the propagation of the output signal in the destiny detection, and we also overcome it using the method.

2. Model and Hamiltonian

Traditionally, the optomechanical system consists of a Fabry-Perot cavity with one side is movable with the mechanical oscillator as shown in Fig. 1(a). Similarly, as shown in Fig. 1(b), the system could also be realized by WGM microresonator which supports both an optical mode and

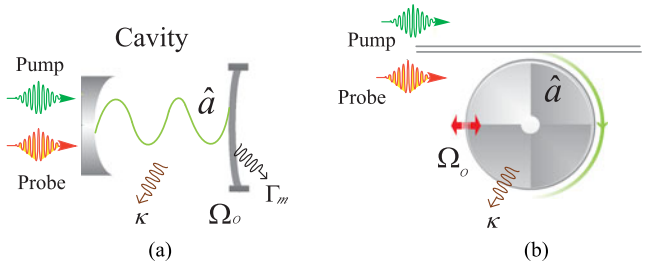

Fig. 1. Schematic diagram of a generic Fabry-Perot and whispering-gallery-mode optomechanical system. The optomechanical system is driven by a strong pump field with frequency ω_1. With a weak probe field ω_p, many strange optical effects occur: optomechanically induced transparency. The intrinsic loss of the cavity is denoted as κ. The coupling strength between the waveguide and cavity is κ_{ex}.

an optomechanical mode. When the system is coherently driven by both the pump and probe field, the Hamiltonian can be written as $\hat{H} = \hat{H}_{mech} + \hat{H}_{opt} + \hat{H}_{int} + \hat{H}_{dirve}$. Here, $\hat{H}_{mech}$ and $\hat{H}_{opt}$ represent the Hamiltonian of the optomechanical field and the cavity field, respectively, which could be described as

$$\hat{H}_{mech} = \frac{\hat{p}^2}{2m_{eff}} + \frac{1}{2} m_{eff} \Omega_m^2 \hat{x}^2 \tag{1}$$

$$\hat{H}_{opt} = \hbar\omega_c \left(\hat{a}^\dagger \hat{a} + \frac{1}{2} \right) \tag{2}$$

where $\hat{p}$ and $\hat{x}$ are the momentum and position operators of the resonator with effective mass m_{eff} and frequency Ω_m, and the cavity mode with the frequency of ω_c is written as the annihilation (creation) operator $\hat{a}(\hat{a}^\dagger)$. The interaction Hamiltonian $\hat{H}_{int}$ is expressed as $\hat{H}_{int} = \hbar G \hat{x} \hat{a}^\dagger \hat{a}$ which describes the interaction between the optical field and the mechanical resonator. $G = \omega_c / L$ denotes the coupling strength with L being the cavity length. $\hat{H}_{dirve}$ represents the Hamiltonian of the input field which consisted of the pump and probe terms as

$$\begin{aligned} \hat{H}_{dirve} = {} & i\hbar\sqrt{\kappa_{ex}} (\varepsilon_1 \hat{a}^\dagger e^{-i\omega_1 t} - \varepsilon_1 \hat{a} e^{j\omega_1 t}) \\ & + i\hbar\sqrt{\kappa_{ex}} (\varepsilon_p \hat{a}^\dagger e^{-i\omega_p t} - \varepsilon_p \hat{a} e^{j\omega_p t}). \end{aligned} \tag{3}$$

Here, κ_{ex} represents the rate of the external loss, and $\omega_1(\omega_p)$ denotes the frequency of the pump(probe) light with amplitude ε_1 (ε_p). Here, we have $\varepsilon_1 = \sqrt{P_1/\hbar\omega_1}$ and $\varepsilon_p = \sqrt{P_p/\hbar\omega_p}$. Respectively, P_1 and P_p are the power of the pump and probe field.

In the frame rotating at the pump field frequency ω_1, the Heisenberg-Langevin equations of the system could be written as

$$\frac{d\hat{a}}{dt} = \left(i\Delta - \frac{\kappa}{2} - iG\hat{x} \right) \hat{a} + \sqrt{\kappa_{ex}} (\varepsilon_1 + \varepsilon_p e^{-i\Omega t}) + \sqrt{\kappa_0} \hat{s}_{vac} \tag{4}$$

$$\frac{d^2\hat{x}}{dt^2} + \Gamma_m \frac{d\hat{x}}{dt} + \Omega_m^2 = -\frac{\hbar G}{m_{eff}} \hat{a}^\dagger \hat{a} + \hat{F}_{th} \tag{5}$$

where $\Delta = \omega_1 - \omega_c$, and $\Omega = \omega_p - \omega_1$. Here, we introduced the decay rate of the cavity field (κ) and mechanical oscillator (Γ_m) classically. The quantum noise of the mechanical oscillator and cavity are denoted as $\hat{F}_{th}$ and $\hat{s}_{vac}$, with $\langle \hat{s}_{vac}(t), \hat{s}^+_{vac}(t') \rangle = \delta(t - t')$, $\langle \hat{s}_{vac}(t) \rangle = 0$, $\langle \hat{F}_{th}(t) \hat{F}^+_{th}(t') \rangle = \Gamma_m$, and $\langle \hat{F}_{th}(t) \rangle = 0$. In this work, the mean field approximation works, viz., $a(t) \equiv \langle \hat{a}(t) \rangle$, $a^*(t) \equiv \langle \hat{a}^+(t) \rangle$ and $x(t) \equiv \langle \hat{x}(t) \rangle$.

Based on these approximations, by neglecting the quantum noise under the strong classical exciting condition, the mean value of the Heisenberg-Langevin equations can be written in the

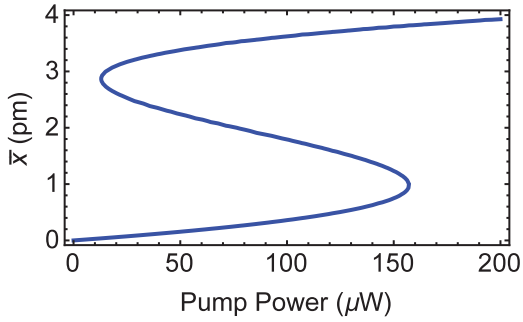

Fig. 2. Calculation results of the solutions of (8). Here, we shows the affect of pump power P_1. We use $m_{eff} = 2.0$ pg, $G = -485$ GHz/nm, $\Gamma_m/2\pi = 35.0$ kHz, $\kappa/2\pi = 50.0$ MHz, $\kappa_{ex}/2\pi = 25.0$ MHz, and $\Omega_m = 1.4$ GHz.

c-number form as

$$\frac{da}{dt} = \left(i\Delta - \frac{\kappa}{2} - iGx\right)a + \sqrt{\kappa_{ex}}(\varepsilon_1 + \varepsilon_p e^{-i\Omega t}) \tag{6}$$

$$\frac{d^2x}{dt^2} + \Gamma_m \frac{dx}{dt} + \Omega_m^2 = -\frac{\hbar G}{m_{eff}} a^* a. \tag{7}$$

For the case that the probe field is much weaker than the pump field, the perturbation method is employed to address the issue of the above equations. The expression of the cavity field and the mechanical displacement under both the pump field and the probe field can be written as $a = \bar{a} + \delta a$ and $x = \bar{x} + \delta x$, and the steady state solution of the above equations could be solved as

$$\bar{a} = \frac{\sqrt{\kappa_{ex}} a_{in}}{-i\bar{\Delta} + \kappa/2}, \quad \bar{x} = \frac{\hbar G\,|\bar{a}|^2}{m_{eff}\Omega_m^2} \tag{8}$$

where $\bar{\Delta} = \omega_1 - (\omega_c + G\bar{x})$ represents the effective detuning of cavity resonance. Consider the case that the pump laser is tuned close to the lower sideband, i.e., $\bar{\Delta} \approx -\Omega_m$, and we choose the system parameters as [42], $m_{eff} = 2.0$ pg, $G = -485$ GHz/nm, $\Gamma_m/2\pi = 35.0$ kHz, $\kappa/2\pi = 50.0$ MHz, $\kappa_{ex}/2\pi = 25.0$ MHz and $\Omega_m = 1.4$ GHz, the displacement $\bar{x}$ exhibits the bistable properties along with the variances of the control field which is shown in Fig. 2. The pump wavelength is chosen to be $\lambda = 530$ nm, we find that when $P_1 < 300$ μW, the displacement of mechanical oscillation is $\bar{x} < 5$ pm and $G\bar{x} \ll \Omega_m$. When $P_1 < 10$ μW or $P_1 > 150$ μW, only one solution of the equation exists. Here in this study, we choose the pump power as $P_1 = 7.3$ μW in order to avoid the bistable effect.

Considering the perturbation part, we use the following ansatz as [15]

$$\delta\hat{a}(t) = A^- e^{-i\Omega t} + A^+ e^{+i\Omega t} \tag{9}$$

$$\delta\hat{a}^*(t) = (A^+)^* e^{-i\Omega t} + (A^-)^* e^{+i\Omega t} \tag{10}$$

$$\delta x(t) = X e^{-i\Omega t} + X^* e^{+i\Omega t}. \tag{11}$$

The radiation-pressure force will oscillate at the beat frequency $\Omega = \omega_p - \omega_1$ with the simultaneous presence of pump and probe fields. When the beat frequency (Ω) is closed to the frequency Ω_m, the mechanical mode starts to oscillate coherently which induces the stokes (A^+) and anti-Stokes scattering of light from the strong intracavity field. By substituting (9)–(11) into (6) and (7), and the

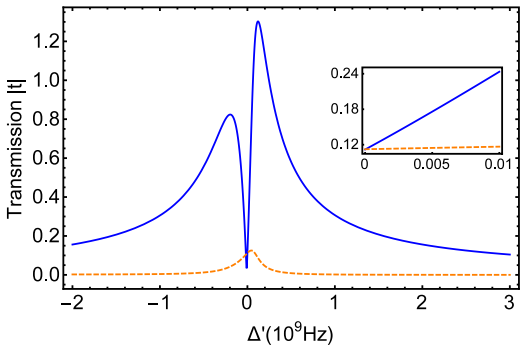

Fig. 3. Transmission of Stokes and homodyne signal with the parameters $m_{eff} = 2.0$ pg, $G = -485$ GHz/nm, $\Gamma_m/2\pi = 35.0$ kHz, $\kappa/2\pi = 100.0$ MHz, $\kappa_{ex}/2\pi = 25.0$ MHz, and $\Omega_m = 1.4$ GHz. Blue solid line shows the transmission of homodyne signal t_{hom}, and the orange dash line shows the transmission of the stokes field t^+.

probe frequency $\omega_1 + \Omega$ term, we can get the equations of A^- and A^+ as

$$(-i(\overline{\Delta} + \Omega) + \kappa/2)A^- = -iG\bar{a}X + \sqrt{\kappa_{ex}}s_p \tag{12}$$

$$(i(\overline{\Delta} - \Omega) + \kappa/2)(A^+)^* = iG\bar{a}X \tag{13}$$

$$m_{eff}(\Omega_m^2 - \Omega^2 - i\Gamma_m\Omega) = -\hbar G\bar{a}(A^- + (A^+)^*). \tag{14}$$

The solution of these equations could be expressed as

$$(A^+)^* = -\frac{if(\Omega_m)}{-i(\overline{\Delta} + \Omega) + \kappa/2 + 2\overline{\Delta}f(\Omega_m)}\sqrt{\kappa_{ex}}s_p \tag{15}$$

$$A^- = \frac{1 + if(\Omega_m)}{-i(\overline{\Delta} + \Omega) + \kappa/2 + 2\overline{\Delta}f(\Omega_m)}\sqrt{\kappa_{ex}}s_p \tag{16}$$

with

$$f(\Omega_m) = \hbar G^2\bar{a}^2\frac{\chi(\Omega_m)}{i(\overline{\Delta} + \Omega) + \kappa/2} \tag{17}$$

$$\chi(\Omega_m) = \frac{1}{m_{eff}}\frac{1}{\Omega_m^2 - \Omega^2 - i\Omega\Gamma_m}. \tag{18}$$

Exploiting the input-output relation of the cavity, the transmission spectrum of the Stokes (t^+) field and OMIT spectrum (t^-) could be written as

$$t^+ = t_{2\omega_1 - \omega_p} = \frac{-if(\Omega_m)\kappa_{ex}}{-i(\overline{\Delta} + \Omega) + \kappa/2 + 2\overline{\Delta}f(\Omega_m)} \tag{19}$$

$$t^- = t_{\omega_p} = 1 - \frac{(1 + if(\Omega_m))\kappa_{ex}}{-i(\overline{\Delta} + \Omega) + \kappa/2 + 2\overline{\Delta}f(\Omega_m)}. \tag{20}$$

For the OMIT signal using under the homodyne detection, we can get [30]

$$t_{hom} \approx 1 - t^- = \frac{[1 + if(\Omega_m)]\kappa_{ex}}{-i(\overline{\Delta} + \Omega) + \kappa/2 + 2\overline{\Delta}f(\Omega_m)} \tag{21}$$

where the intracavity probe power with frequency $2\omega_l - \omega_p$ could be detected from the homodyne signal.

In Fig. 3, we plot the transmission spectrum of Stokes and homodyne signal field with different Δ', where $\Delta' = \Omega - \Omega_m$. In the OMIT windows area, the Stokes filed can not be neglected, as shown in

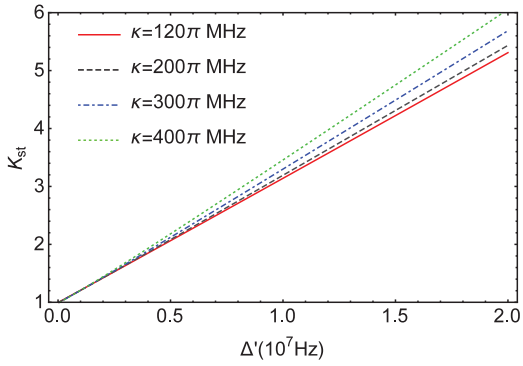

Fig. 4. Results of K_{st} in (24). Here, we show the effect of pump power P_1, and we set the parameters as $m_{eff} = 2.0$ pg, $G = -485$ GHz/nm, $\Gamma_m/2\pi = 35.0$ kHz, $\kappa_{ex}/2\pi = 50.0$ MHz, and $\Omega_m = 1.4$ GHz.

the subgraph of Fig. 3. We find that the stokes is equal to the intensity of the homodyne signal. Then the homodyne signal intensity varies directly with the effective mass of the mechanical resonator (or strictly, decrease of the mechanical resonator's frequency). Then, the change of the effective mass of the mechanical resonator could be mapped onto the change of output signal intensity. We take the stokes signal as a reference in order to eliminate the decay in signal propagation. The Stokes signal and homodyne signal have a negligible frequency difference simultaneously, they can create at almost the same time in the optical cavity. Therefore, they will undergo the same decay when the environment is linear and have frequency irrelevant dissipation.

3. Nanomechiancal Mass Sensing Using OMIT

In in this part, we give a detailed analysis of the mass sensing process based on the Stokes signal in the nanomechanical system.

3.1. Nanomechiancal Frequency Shift and Amplitude Variation

In order to achieve mass sensing, we first consider the relationship between the output signals and the nanomechanical frequency shift. Here, we suggest that the output Stokes and homodyne signals have a frequency irrelevant dissipation symbols by $\gamma(t)$; then, the power of the detection can be written as

$$t'_{hom} = \int t_{hom} e^{-i\gamma(t_1)t_1} dt_1 \tag{22}$$

$$t'^{+} = \int t^{+} e^{-i\gamma(t_2)t_2} dt_2. \tag{23}$$

Consider that the detuning between the Stokes signal and homodyne signal is twice of the mechanical resonator level, the dispersion could be ignored. Meanwhile, we can set $t_1 = t_2$ for the wavefront of these two signals are always coincident. The t_{hom} and t^{+} signal are time irrelevant and we can define the relative intensity (K_{st}) as

$$K_{st} = \left|\frac{t'_{hom}}{t'^{+}}\right| = \left|\frac{\int t_{hom} e^{-i\gamma(t_1)t_1} dt_1}{\int t^{+} e^{-i\gamma(t_2)t_2} dt_2}\right|$$

$$= \left|\frac{t_{hom} \int e^{-i\gamma(t)t} dt}{t^{+} \int e^{-i\gamma(t)t} dt}\right| = \left|\frac{t_{hom}}{t^{+}}\right| = \left|1 + \frac{1}{if(\Omega_m)}\right|. \tag{24}$$

As shown in (24), by using the relative value of the homodyne and stokes signals, the mathematical form is also simplified by comparing with the form of homodyne signal and stokes signal.

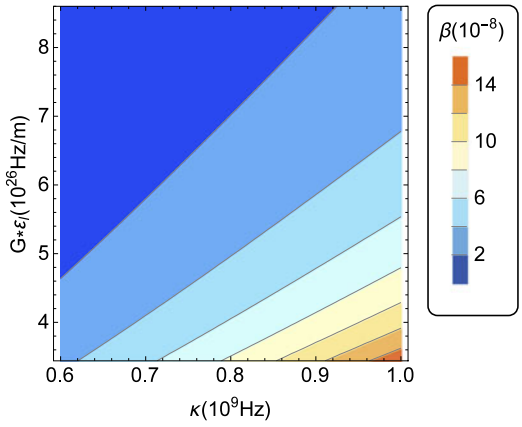

Fig. 5. Relative intensity of β under different κ and $G\epsilon_l$, with $m_{eff} = 2.0$ pg, $\Gamma_m/2\pi = 35.0$ kHz, $\kappa_{ex}/2\pi = 50.0$ MHz, pump power 7 μW with wavelength $\lambda = 532$ nm, and $\Omega_m = 1.4$ GHz.

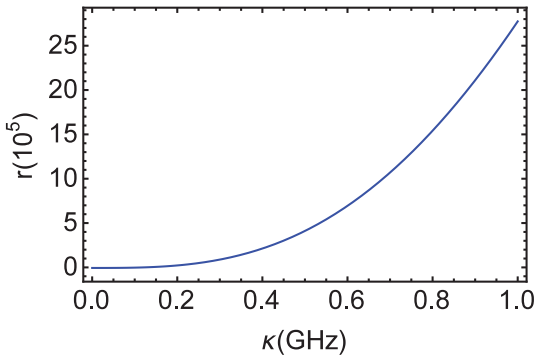

Fig. 6. r under different κ with $m_{eff} = 2.0$ pg, $\Gamma_m/2\pi = 35.0$ kHz, $\kappa_{ex}/2\pi = 50.0$ MHz, pump power 7 μW with wavelength $\lambda = 532$ nm, and $\Omega_m = 1.4$ GHz

In Fig. 4, we plot the relative intensity K_{st} with different frequency shift ($\delta\Omega_m = \Delta'$) under different decay rate (κ). Here we keep the system always under the critical coupling condition which means the coupling rate is related with the cavity decay rate, and we can conclude that there is a direct proportional relationship between the frequency shift($\delta\Omega_m$) and K_{st}. Therefore, the frequency can be easily read out from the variation of the relative intensity. According to the increment of the decay rate (κ), the relative intensity is more sensitive than the frequency shift.

3.2. Mass Sensor Under Different Parameters

As shown in Fig. 3, the power of the Stokes signal is equal to the homodyne signal at $\Delta' = 0$. There we assume that the system is tuned to resonant with the frequency of the probe field. The frequency shift will happen due to the deposition of the nanoparticle on the mechanical system. Based on the relationship between the effective mass m_{eff}, spring constant k and the fundamental resonance frequency [43] $\Omega_m = \sqrt{k/m_{eff}}$, the mass change ($m_d$) of the mechanical resonator can be numerically solved as [44]

$$\frac{\delta\Omega_m}{m_d} = \frac{\Omega_m}{\partial m_{eff}} = -\frac{\Omega_m}{2m_{eff}} \tag{25}$$

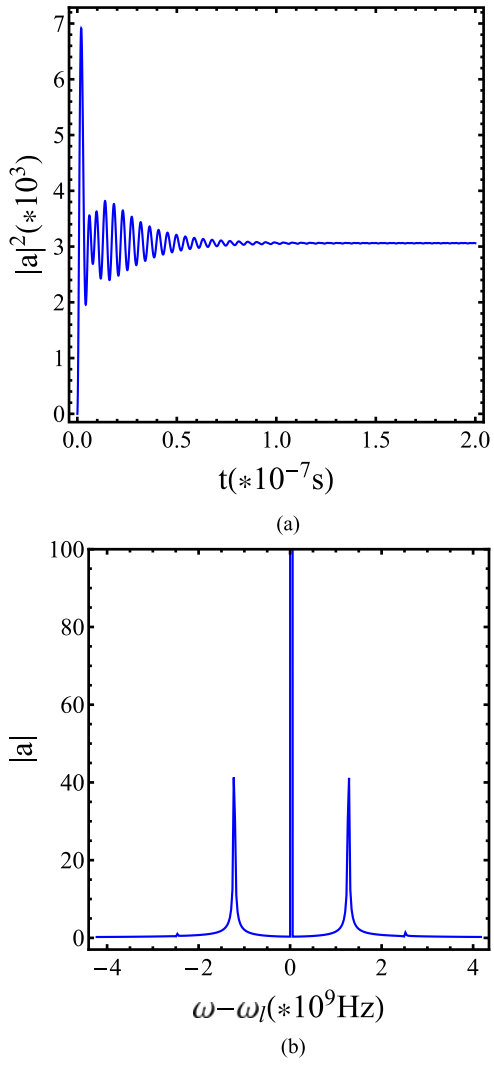

Fig. 7. Numerical simulation of the mass sensing spectrum on the frequency domain. Here, we use the parameter as $m_{eff} = 2.0$ pg, $G = -485$ GHz/nm, $\Gamma_m/2\pi = 35.0$ kHz, $\kappa/2\pi = 100.0$ MHz, $\kappa_{ex}/2\pi = 25.0$ MHz, and $\Omega_m = 1.4$ GHz. Pump power $P_{pu} = 7.3$ μW, and probe power $P_{pr} = 7.3$ nW.

The relation between m_d and K_{st} could be described as

$$K_{st} = \left| 1 + \frac{1}{if(\Omega_{m+m_d})} \right|. \tag{26}$$

Moreover, we define β as the slope of the K_{st} value, which can be express as

$$\beta = \frac{dK_{st}(m_{eff})}{dm_d} \tag{27}$$

which reveals the relationship between the relative amplitude of the field and the mass change. Here we numerically simulated the value of β under different κ and $G\varepsilon_l$ in Fig. 5. What should be noticed is that, ε_l determines the steady state of the system which is related with the pumping field. However, the destiny of the Stokes and homodyne signals are mainly determined by the probe field. In Fig. 5, we found that the slope of β will be increased along with the increment of κ or with the decrement of $G\varepsilon_l$.

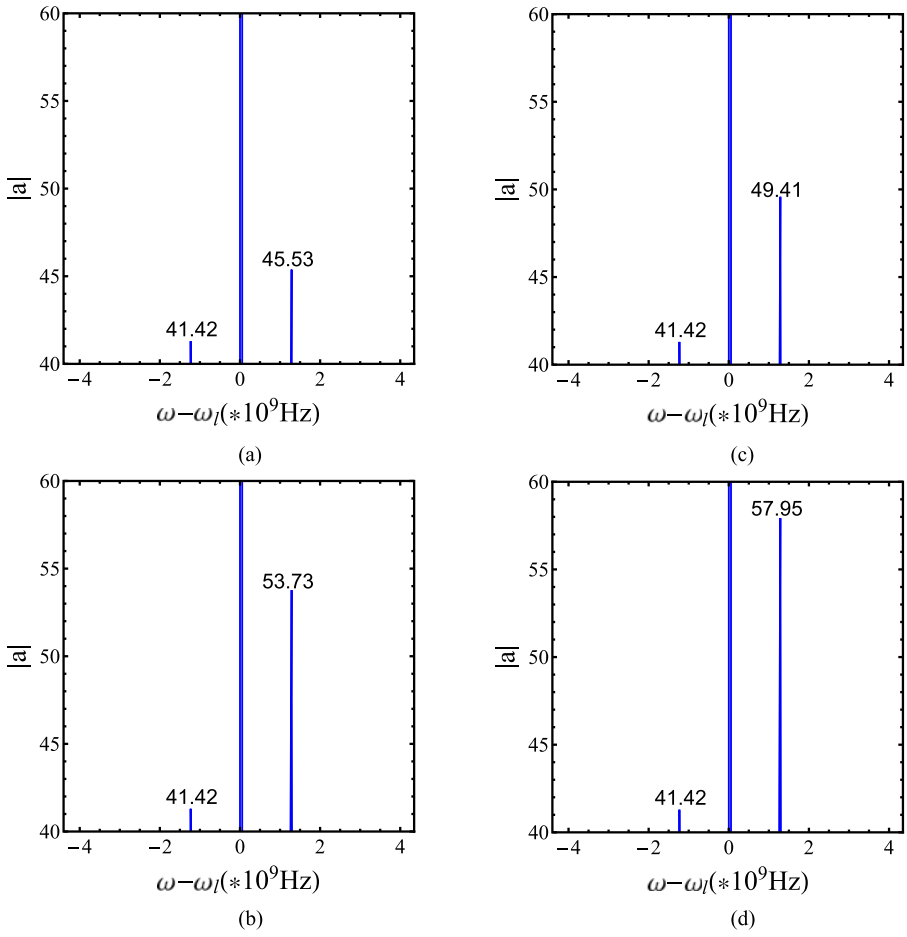

Fig. 8. Numerical simulation of the mass sensing spectrum on time domain and frequency domain. Here, we use the parameter as $m_{eff} = 2.0$ pg, $G = -485$ GHz/nm, $\Gamma_m/2\pi = 35.0$ kHz, $\kappa/2\pi = 100.0$ MHz, $\kappa_{ex}/2\pi = 25.0$ MHz, and $\Omega_m = 1.4$ GHz. The pump power $P_{pu} = 7.3$ μW, and probe power $P_{pr} = 7.3$ nW. (a) Time evaluation of the cavity field of bare nano-resonator. (b) Frequency spectrum of the cavity field of bare nano-resonator.

In order to ensure the system works in the direct proportional area, the second order term should be much smaller than the first order term ($r = K'_{st}/K''_{st} \gg 1$). We find that term $G\varepsilon_l$ will have no affect on this requirement, but κ works. In Fig. 6, we plot the relationship between the first parameter of r and κ. This graph shows that the direct proportional relationship is maintained when the decay rate(κ) is greater than 0.1 GHz.

3.3. The Frequency Spectrum of Mass Sensing

In this part, we will illustrate the measurement process using this system. The detailed operations could be described as follows: 1) The frequency of the pump field is tuned to locate in the transparency window of OMIT. 2) When the probe field is sent into the system, after reaching the steady state, the field amplitude of the stokes and homodyne signals should be readout and the relative amplitude could be calculated. 3) Mass change of the nano-resonator induced by nanoparticle will have a slight change on the intensity, and the variance of the relative amplitude could be detected. 4) Read out of the mass according to the relationship between m_d and K_{st}, as shown in Fig. 5 or (26).

As shown in Fig. 7, we plot the time domain evolution and the steady state frequency spectrum of the optical field. Here we can find the system reach its steady state in about 70 ns from Fig. 7(a), which means the mass sensing can be achieved in a quiet short time. Also we can get the reference of zero point. The Stokes and homodyne signals have almost the same amplitude in this point. Based on the zero point value, we can get the added mass on the nanomechancial according to the relative amplitude change.

As shown in Fig. 8, we simulate the behavior of the output signal with the variation of the different nanoparticles with the mass of $\{1.428, 2.857, 4.287, 5.671\}$ fg on the nanomechanical resonators, and the output signal exhibits significant variations. As shown in Fig. 8, we find that the homodyne signal shows different values of 45.53, 49.41, 53.75, 57.95, and the Stokes signal keeps unchanged with the value of 41.42. Based on the corresponding relationship between K_{st} and m_d shown in Fig. 5 and (26). The sensing mass based on the simulation can be read as $\{1.323, 2.572, 3.962, 5.321\}$ fg. We may find there is a slight difference of 14%. This error may be induced by the nonlinear effect of the pump field which increases the value of the homodyne and stokes field, then the simulation value of the K_{st} would be smaller. We can find the detection mass can be written as $\{1.410, 2.741, 4.223, 5.671\}$ fg. Then, the maximal errors will reduce to 3%. Here we assume the photon-detector at photon level as $(|a| + \delta|a|)^2 - |\delta|^2 = 1$. Consider the strength shown in Fig.(8), we take $|a| = 40$. Then we can get $\delta a = 0.0125$. This corresponds to a mess value of 4 ag.

4. Summary

In summary, we have present a stokes reference method to achieve mass sensing based on the intensity measurement of the output frequency spectrum. We provide an expression to describe the added mass of the nano-resonator. We also discussed the performance of the mass sensing under different system parameters in the numerical simulation. We find that at least the massing of femtogram sensing can be achieved even the cavity is Low-Q and the coupling is not strong enough.

References

[1] P. S. Waggoner and H. G. Craighead, "Micro-and nanomechanical sensors for environmental, chemical, and biological detection," *Lab Chip*, vol. 7, pp. 1238–1255, 2007.
[2] H. G. Craighead, "Nanoelectromechanical systems," *Science*, vol. 290, pp. 1532–1535, 2000.
[3] K. L. Ekinci and M. L. Roukes, "Nanoelectromechanical systems," *Rev. Sci. Instrum.*, vol.76, 2005, Art. no. 061101.
[4] N. V. Lavrik, M. J. Sepaniak, and P. G. Datskos, "Cantilever transducers as a platform for chemical and biological sensors," *Rev. Sci. Instrum.*, vol. 75, pp. 2229–2253, 2004.
[5] B. Ilic, H. Craighead, S. Krylov, W. Senaratne, C. Ober, and P. Neuzil, "Attogram detection using nanoelectromechanical oscillators," *J. Appl. Phys.*, vol. 95, pp. 3694–3703, 2004.
[6] M. W. Pruessner, T. H. Stievater, M. S. Ferraro, W. S. Rabinovich, J. L. Stepnowski, and R. A. McGill, "Waveguide micro-opto-electro-mechanical resonant chemical sensors," *Lab Chip*, vol. 10, pp. 762–768, 2010.
[7] J. Zhu *et al.*, "On-chip single nanoparticle detection and sizing by mode splitting in an ultrahigh-q microresonator," *Nature Photon.*, vol. 4, pp. 46–49, 2010.
[8] L. He, S. K. Özdemir, J. Zhu, W. Kim, and L. Yang, "Detecting single viruses and nanoparticles using whispering gallery microlasers," *Nature Nanotechnol.*, vol. 6, pp. 428–432, 2011.
[9] S. K. Özdemir *et al.*, "Highly sensitive detection of nanoparticles with a self-referenced and self-heterodyned whispering-gallery raman microlaser," in *Proc. Nat. Acad. Sci.*, 2014, vol. 111, pp. E3836–E3844.
[10] B. B. Li, W. R. Clements, X. C. Yu, K. Shi, Q. H. Gong, and Y. F. Xiao, "Single nanoparticle detection using split-mode microcavity raman lasers," in *Proc. Nat. Acad. Sci.*, 2014, vol. 111, pp. 14657–14662.
[11] F. Vollmer and S. Arnold, "Whispering-gallery-mode biosensing: Label-free detection down to single molecules," *Nature Methods*, 2008, vol. 5, pp. 591–596.
[12] X. C. Yu *et al.*, "Single nanoparticle detection and sizing using a nanofiber pair in an aqueous environment," *Adv. Mater.*, vol. 26, pp. 7462–7467, 2014.
[13] B. Q. Shen *et al.*, "Detection of single nanoparticles using the dissipative interaction in a high-q microcavity," *Phys. Rev. Appl.*, vol. 5, 2016, Art. no. 024011.
[14] C. Wang, Q. Quan, S. Kita, Y. Li, and M. Lončar, "Single-nanoparticle detection with slot-mode photonic crystal cavities," *Appl. Phys. Lett.*, vol. 106, 2015, Art. no. 261105.
[15] T. J. Kippenberg and K. J. Vahala, "Cavity opto-mechanics," *Opt. Exp.*, vol. 15, pp. 17172–17205, 2007.
[16] F. Marquardt and S. M. Girvin, "Optomechanics (a brief review)," arXiv:0905.0566, 2009.

[17] T. J. Kippenberg and K. J. Vahala, "Cavity optomechanics: Back-action at the mesoscale," *Science*, vol. 321, pp. 1172–1176, 2008.
[18] J. Chan *et al.*, "Laser cooling of a nanomechanical oscillator into its quantum ground state," *Nature*, vol. 478, pp. 89–92, 2011.
[19] A. H. Safavi-Naeini *et al.*, "Electromagnetically induced transparency and slow light with optomechanics," *Nature*, vol. 472, pp. 69–73, 2011.
[20] C. Doolin, P. H. Kim, B. D. Hauer, A. J. R. MacDonald, and J. P. Davis, "Multidimensional optomechanical cantilevers for high-frequency force sensing," *New J. Phys.*, vol. 16, 2014, Art. no. 035001.
[21] I. Wilson-Rae, P. Zoller, and A. Imamoğlu, "Laser cooling of a nanomechanical resonator mode to its quantum ground state," *Phys. Rev. Lett.*, vol. 92, 2004, Art. no. 075507.
[22] J.-J. Li and K.-D. Zhu, "Weighing a single atom using a coupled plasmonic-carbon nanotube system," *Sci. Technol. Adv. Mater.*, vol. 13, 2012, Art. no. 025006.
[23] I. Yeo *et al.*, "Strain-mediated coupling in a quantum dot-mechanical oscillator hybrid system," *Nature Nanotechnol.*, vol. 9, pp. 106–110, 2014.
[24] J. Chaste, A. Eichler, J. Moser, G. Ceballos, R. Rurali, and A. Bachtold, "Nanomechanical mass sensor with yoctogram resolution," *Nature Nanotechnol.*, vol. 7, pp. 301–304, 2012.
[25] K. Jensen, K. Kim, and A. Zettl, "An atomic-resolution nanomechanical mass sensor," *Nature Nanotechnol.*, vol. 3, pp. 533–537, 2008.
[26] J.-J. Li and K.-D. Zhu, "Nonlinear optical mass sensor with an optomechanical microresonator," *Appl. Phys. Lett.*, vol. 101, 2012, Art. no. 14 1905.
[27] F. Liu, S. Alaie, Z. C. Leseman, and M. Hossein-Zadeh, "Sub-pg mass sensing and measurement with an optomechanical oscillator," *Opt. Exp.*, vol. 21, pp. 19555–19567, 2013.
[28] K. H. Kim and X. Fan, "Surface sensitive microfluidic optomechanical ring resonator sensors," *Appl. Phys. Lett.*, vol. 105, 2014, Art. no. 191101.
[29] Y. He, "Sensitivity of optical mass sensor enhanced by optomechanical coupling," *Appl. Phys. Lett.*, vol. 106, 2015, Art. no. 12 1905.
[30] S. Weis *et al.*, "Optomechanically induced transparency," *Science*, vol. 330, pp. 1520–1523, 2010.
[31] A. Kronwald and F. Marquardt, "Optomechanically induced transparency in the nonlinear quantum regime," *Phys. Rev. Lett.*, vol. 111, 2013, Art. no. 133601.
[32] H. Xiong, L.-G. Si, A.-S. Zheng, X. Yang, and Y. Wu, "Higher-order sidebands in optomechanically induced transparency," *Phys. Rev. A*, vol. 86, 2012, Art. no. 013815.
[33] G. S. Agarwal and S. Huang, "Electromagnetically induced transparency in mechanical effects of light," *Phys. Rev. A*, vol. 81, 2010, Art. no. 04 1803.
[34] P.-C. Ma, J.-Q. Zhang, Y. Xiao, M. Feng, and Z.-M. Zhang, "Tunable double optomechanically induced transparency in an optomechanical system," *Phys. Rev. A*, vol. 90, 2014, Art. no. 043825.
[35] M. Aspelmeyer, T. J. Kippenberg, and F. Marquardt, "Cavity optomechanics," *Rev. Mod. Phys.*, vol. 86, pp. 1391–1452, 2014.
[36] K.-J. Boller, A. Imamoğlu, and S. E. Harris, "Observation of electromagnetically induced transparency," *Phys. Rev. Lett.*, vol. 66, pp. 2593–2596, 1991.
[37] Z. Duan, B. Fan, T. M. Stace, G. J. Milburn, and C. A. Holmes, "Induced transparency in optomechanically coupled resonators," *Phys. Rev. A*, vol. 93, 2016, Art. no. 023802.
[38] F. Marquardt, J. G. E. Harris, and S. M. Girvin, "Dynamical multistability induced by radiation pressure in high-finesse micromechanical optical cavities," *Phys. Rev. Lett.*, vol. 96, 2006, Art. no. 103901.
[39] A. Schliesser, R. Rivieére, G. Anetsberger, O. Arcizet, and T. J. Kippenberg, "Resolved-sideband cooling of a micromechanical oscillator," *Nature Phys.*, vol. 4, pp. 415–419, 2008.
[40] C. Cao, S. C. Mi, T. J. Wang, R. Zhang, and C. Wang, "Optical high-order sideband comb generation in a photonic molecule optomechanical system," *IEEE J. Quantum Electron.*, vol. 52, no. 6, pp. 1–5, Jun. 2016.
[41] C. Cao *et al.*, "Tunable high-order sideband spectra generation using a photonic molecule optomechanical system," *Sci. Rep.*, vol. 6, 2016, Art. no. 22920.
[42] L. Ding *et al.*, "Wavelength-sized gaAs optomechanical resonators with gigahertz frequency," *Appl. Phys. Lett.*, vol. 98, 2011, Art. no. 113108.
[43] B. Lassagne, D. Garcia-Sanchez, A. Aguasca, and A. Bachtold, "Ultrasensitive mass sensing with a nanotube electromechanical resonator," *Nano Lett.*, vol. 8, pp. 3735–3738, 2008.
[44] Y. He and M. P. Jiang, "Ultrasensitive mass sensing method based on slow light in cavity optomechanics," *Appl. Phys. Exp.*, vol. 9, no. 5, 2016, Art. no. 052205.